

Tensor Neural Network and Its Numerical Integration^{*}

Yifan Wang[†], Pengzhan Jin[‡], and Hehu Xie[§]

Abstract

In this paper, we introduce a type of tensor neural network. For the first time, we propose its numerical integration scheme and prove the computational complexity to be the polynomial scale of the dimension. Based on the tensor product structure, we develop an efficient numerical integration method by using fixed quadrature points for the functions of the tensor neural network. The corresponding machine learning method is also introduced for solving high-dimensional problems. Some numerical examples are also provided to validate the theoretical results and the numerical algorithm.

Keywords. Tensor neural network, numerical integration, fixed quadrature points, machine learning, high-dimensional eigenvalue problem.

AMS subject classifications. 65N30, 65N25, 65L15, 65B99

1 Introduction

Partial differential equations (PDEs) appear in many scientific and industrial applications since they can describe physical and engineering phenomena or processes. So far, many types of numerical methods have been developed such as the finite difference method, finite element method, and spectral method for solving PDEs in three spatial dimensions plus the temporal dimension. But there exist many high-dimensional PDEs such as many-body Schrödinger, Boltzmann equations, Fokker-Planck equations, and stochastic PDEs (SPDEs), which are almost impossible to be solved using traditional numerical methods. Recently, many numerical methods have been proposed based on machine learning to solve the high-dimensional PDEs ([1, 5, 6, 14, 25, 26, 30, 35, 36]). Among these machine learning methods, neural network-based methods attract more and more attention. Neural networks can be used to build approximations of the exact solutions of PDEs by machine

^{*}This work was supported in part by the National Key Research and Development Program of China (2019YFA0709601), the National Center for Mathematics and Interdisciplinary Science, CAS.

[†]LSEC, NCMIS, Institute of Computational Mathematics, Academy of Mathematics and Systems Science, Chinese Academy of Sciences, Beijing 100190, China, and School of Mathematical Sciences, University of Chinese Academy of Sciences, Beijing 100049, China (wangyifan@lsec.cc.ac.cn).

[‡]School of Mathematical Sciences, Peking University, Beijing 100871, China (jpz@pku.edu.cn).

[§]LSEC, NCMIS, Institute of Computational Mathematics, Academy of Mathematics and Systems Science, Chinese Academy of Sciences, Beijing 100190, China, and School of Mathematical Sciences, University of Chinese Academy of Sciences, Beijing 100049, China (hhxie@lsec.cc.ac.cn).

learning methods. The reason is that neural networks can approximate any function given enough parameters. This type of method provides a possible way to solve many useful high-dimensional PDEs from physics, chemistry, biology, engineering, and so on.

Due to its universal approximation property, the fully-connected neural network (FNN) is the most widely used architecture to build the functions for solving high-dimensional PDEs. There are several types of FNN-based methods such as well-known the deep Ritz [6], deep Galerkin method [35], PINN [30], and weak adversarial networks [36] for solving high-dimensional PDEs by designing different loss functions. Among these methods, the loss functions always include computing high-dimensional integration for the functions defined by FNN. For example, the loss functions of the deep Ritz method require computing the integrations on the high-dimensional domain for the functions which is constructed by FNN. Direct numerical integration for the high-dimensional functions also meets the “curse of dimensionality”. Always, the Monte-Carlo method is adopted to do the high-dimensional integration with some types of sampling methods [6, 15]. Due to the low convergence rate of the Monte-Carlo method, the solutions obtained by the FNN-based numerical methods are difficult to obtain high accuracy and stable convergence process. In other words, the Monte-Carlo method decreases computational work in each forward propagation by decreasing the simulation efficiency and stability of the FNN-based numerical methods for solving high-dimensional PDEs.

The CANDECOMP/PARAFAC (CP) tensor decomposition builds a low-rank approximation method and is a widely used way to cope with the curse of dimensionality. The CP method decomposes a tensor as a sum of rank-one tensors which can be considered as the higher-order extensions of the singular value decomposition (SVD) for the matrices. This means the SVD idea can be generalized to the decomposition of the high-dimensional Hilbert space into the tensor product of several Hilbert spaces. The tensor product decomposition has been used to establish low-rank approximations of operators and functions [4, 12, 20, 31]. If we use the low-rank approximation to do the numerical integration, the computational complexity can avoid the exponential dependence on the dimension in some cases [2, 26]. Inspired by CP decomposition, this paper focuses on a special low-rank neural networks structure and its numerical integration. It is worth mentioning that although CP decomposition should be useful to obtain a low-rank approximation, there is no known general result to give the relationship between the rank (hyperparameter p in this paper) and error bounds. For more details, please refer to [16, 23] and numerical investigations [4].

This paper aims to propose a type of tensor neural network (TNN) to build the trial functions for solving high-dimensional PDEs. The TNN is a function being designed by the tensor product operations on the neural networks or by low-rank approximations of FNNs. An important advantage is that we do not need to use Monte-Carlo method to do the integration for the functions which is constructed by TNN. This is the main motivation to design the TNN for high-dimensional PDEs in this paper. We will show, the computational work for the integration of the functions by TNN is only a polynomial scale of the dimension, which means the TNN overcomes the “curse of dimensionality” in some sense for solving high-dimensional PDEs.

An outline of the paper goes as follows. In Section 2, we introduce the way to build TNN. The numerical integration method for the functions constructed by TNN is designed in Section 3.

Section 4 is devoted to proposing the TNN-based machine learning method for solving the high-dimensional eigenvalue problem with the numerical integration method. Some numerical examples are provided in Section 5 to show the validity and efficiency of the proposed numerical methods in this paper. Some concluding remarks are given in the last section.

2 Tensor neural network architecture

In this section, we introduce the TNN and its approximation property. Without loss of generality, we first design the general TNN architecture with K -dimensional output to accommodate more general computational aims. Then we consider the 1-dimensional output TNN architecture which is our primary focus in this paper. Of course, it is easy to know that the K -dimensional output TNN can also be built with K 1-dimensional output TNN. The approximation property for the 1-dimensional TNN, which will be given in this section, can be directly extended to K -dimensional output TNN.

The architecture of TNN is similar to MIONet, just by setting the Banach spaces to Euclidean spaces, more details about MIONet can be found in [20]. MIONet mainly discusses the approximation of multiple-input continuous operators by low-rank neural network structures and investigates the function approximation under C -norm. The inputs of MIONet are the vectors that denote the coefficients of projections of functions in infinite-dimensional Banach spaces onto the concerned finite-dimensional subspace. While TNN considers solving high-dimensional PDEs and pays more attention to the high-dimensional integration and the approximation to functions in Sobolev space by low-rank neural network structures in H^m -norm. Different from MIONet, the inputs of TNN is a series of integration points in one-dimensional Euclidean space. These points can guarantee high precision and high efficiency in calculating the numerical integrations in the loss function derived from the variational principle. The most important contribution of this paper is to consider the numerical integrations of TNN for solving high-dimensional PDEs with TNN. More specifically, we first construct d subnetworks, where each subnetwork is a continuous mapping from a bounded closed set $\Omega_i \subset \mathbb{R}$ to \mathbb{R}^p . The i -th subnetwork can be expressed as:

$$\Phi_i(x_i; \theta_i) = (\phi_{i,1}(x_i; \theta_i), \phi_{i,2}(x_i; \theta_i), \dots, \phi_{i,p}(x_i; \theta_i))^T, \quad i = 1, \dots, d, \quad (1)$$

where x_i denotes the 1-dimensional input, θ_i denotes the parameters of the i -th subnetwork, typically the weights and biases. The number of layers and neurons in each layer, the selections of activation functions and other hyperparameters can be different in different subnetworks. In this paper, we simply use FNN architectures for each subnetwork. It is worth mentioning that, in addition to FNN, other reasonable architecture can be used as long as it can approximate any mapping from $\Omega_i \subset \mathbb{R}$ to \mathbb{R}^p in some sense. The only thing to be guaranteed is that the output dimensions of these subnetworks should be equal. After building each subnetwork, we combine the output layers of each subnetwork to obtain TNN architecture by the following mapping from \mathbb{R}^d to \mathbb{R}^K

$$\Psi(x; \theta) = W \cdot (\Phi_1(x_1; \theta_1) \odot \Phi_2(x_2; \theta_2) \odot \dots \odot \Phi_d(x_d; \theta_d)), \quad (2)$$

where \odot is the Hadamard product (i.e., element-wise product), Ψ denotes a K -dimensional output function which is defined as $\Psi(x; \theta) = (\Psi_1(x; \theta), \dots, \Psi_K(x; \theta))^T$, the matrix $W \in \mathbb{R}^{K \times p}$ and $x = (x_1, \dots, x_d) \in \Omega_1 \times \dots \times \Omega_d$. In the following part of this paper, we set $\Omega = \Omega_1 \times \dots \times \Omega_d$. Here $\theta = \{\theta_1, \dots, \theta_d, W\}$ denote trainable parameters. Figure 1 shows the architecture of K -dimensional output TNN.

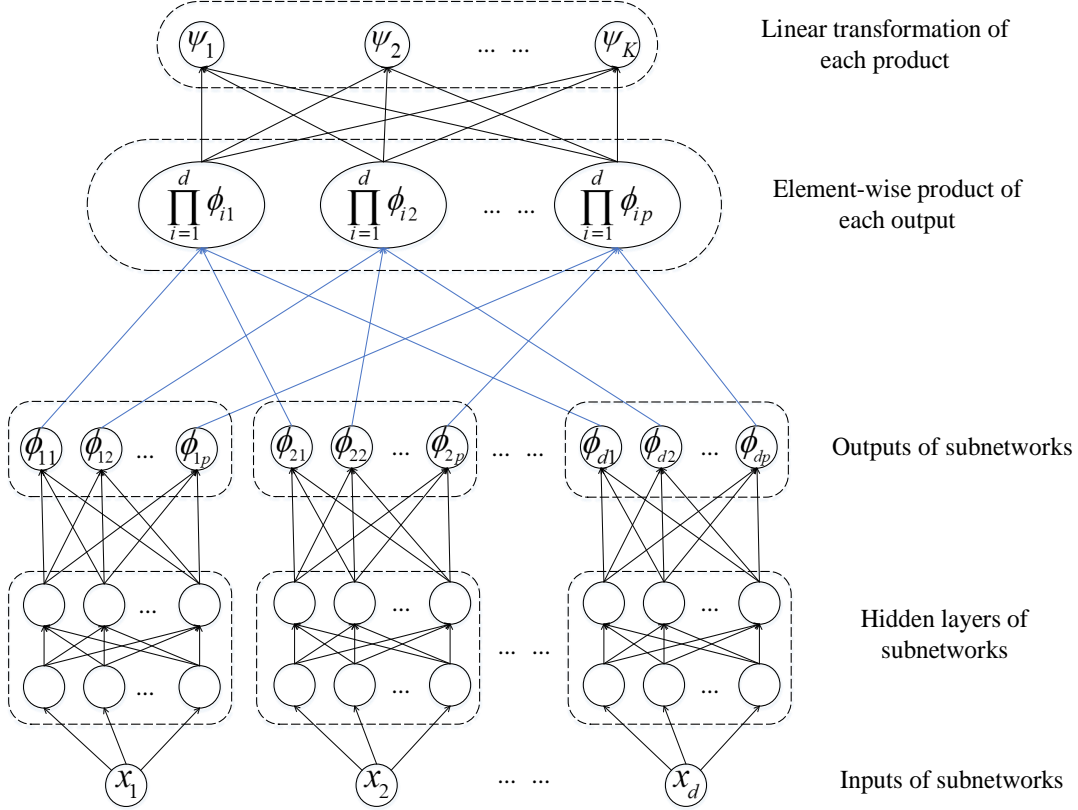


Figure 1: Architecture of K -dimensional output TNN. Black arrows mean linear transformation (or affine transformation). Each ending node of blue arrows is obtained by taking the scalar multiplication of all starting nodes of blue arrows that end in this ending node.

The 1-dimensional output TNN (i.e. $K = 1$) is always enough for solving normal high-dimensional PDEs. When $K = 1$, the matrix W appears in (2) degenerates to a row vector, its members only play the role to scale the components of vectors obtained by the Hadamard product. This effect can also be achieved by scaling the parameters of the output layers of the concerned subnetworks. Therefore, in order to reduce the number of parameters, we set the matrix W to be unity and define the 1-dimensional TNN as follows:

$$\Psi(x; \theta) = \sum_{j=1}^p \phi_{1,j}(x_1; \theta_1) \phi_{2,j}(x_2; \theta_2) \cdots \phi_{d,j}(x_d; \theta_d) = \sum_{j=1}^p \prod_{i=1}^d \phi_{i,j}(x_i; \theta_i), \quad (3)$$

where $\theta = \{\theta_1, \dots, \theta_d\}$ denotes all parameters of the whole architecture. Figure 2 shows the corresponding architecture of 1-dimensional output TNN. For simplicity, TNN refers to the 1-dimensional TNN hereafter in this paper.

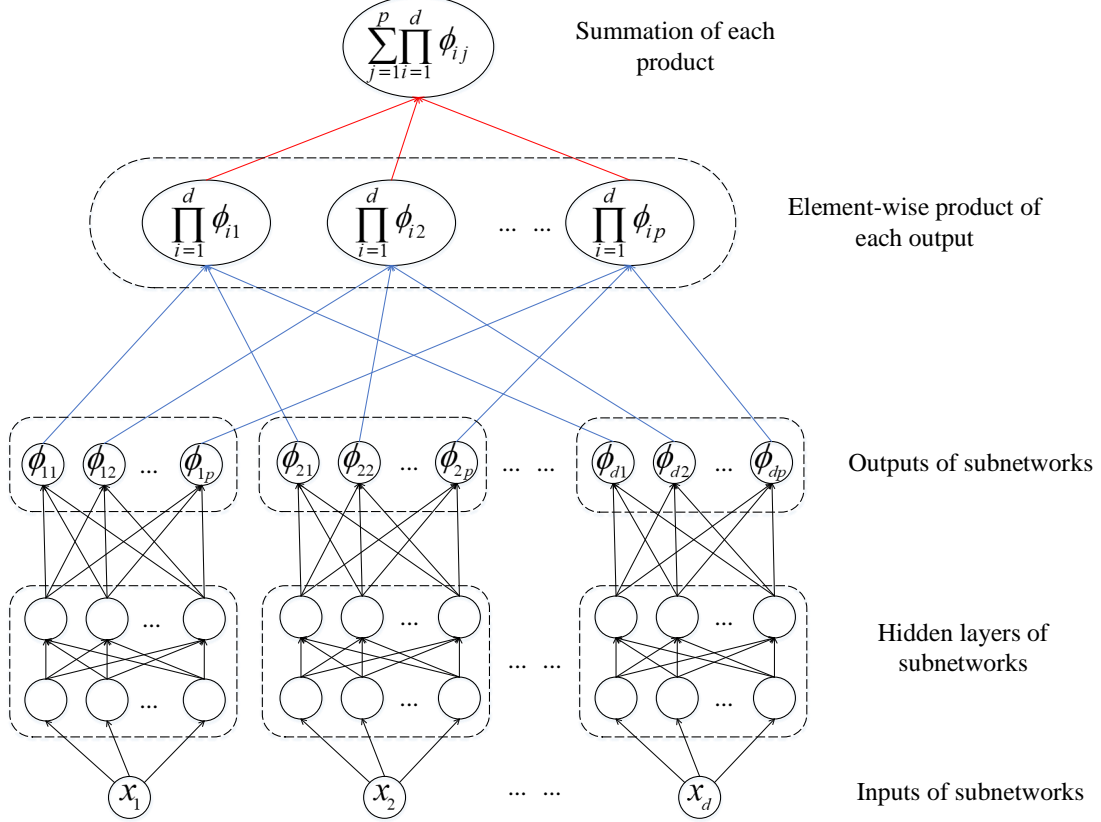


Figure 2: Architecture of 1-dimensional output TNN. Black arrows mean linear transformation (or affine transformation). Each ending node of blue arrows is obtained by taking the scalar multiplication of all starting nodes of blue arrows that end in this ending node. The final output of TNN is derived from summation of all starting nodes of red arrows.

Since there exists the isomorphism relation between $H^m(\Omega_1 \times \dots \times \Omega_d)$ and the tensor product space $H^m(\Omega_1) \otimes \dots \otimes L^2(\Omega_d)$, the process of approximating the function $f(x) \in H^m(\Omega_1 \times \dots \times \Omega_d)$ with the TNN defined by (3) can be regarded as searching for a CP decomposition structure to approximate $f(x)$ in the space $H^m(\Omega_1) \otimes \dots \otimes H^m(\Omega_d)$ with the rank being not greater than p . Due to the low-rank structure, we will find that the polynomial compound acting on the TNN and its derivatives can be integrated with small scale computational work. In order to show the validity for solving PDEs by TNN, we introduce the following approximation result to the functions in the space $H^m(\Omega_1 \times \dots \times \Omega_d)$ under the sense of H^m -norm.

Theorem 1. Assume that each Ω_i is a bounded closed interval in \mathbb{R} for $i = 1, \dots, d$, $\Omega = \Omega_1 \times \dots \times \Omega_d$, and the function $f(x) \in H^m(\Omega)$. Then for any tolerance $\varepsilon > 0$, there exist a positive

integer p and the corresponding TNN defined by (3) such that the following approximation property holds

$$\|f(x) - \Psi(x; \theta)\|_{H^m(\Omega)} < \varepsilon. \quad (4)$$

Proof. Due to the isomorphism relation $H^m(\Omega) \cong H^m(\Omega_1) \otimes \cdots \otimes H^m(\Omega_d)$, for any $\varepsilon > 0$, there exist a positive integer p , $h_{i,j}(x_i) \in H^m(\Omega_i)$, $i = 1, \dots, d$, $j = 1, \dots, p$, and $h(x) \in H^m(\Omega)$ which is defined as follows

$$h(x) = \sum_{j=1}^p h_{1,j}(x_1) \cdots h_{d,j}(x_d) = \sum_{j=1}^p \prod_{i=1}^d h_{i,j}(x_i),$$

such that the following estimate holds

$$\|f(x) - h(x)\|_{H^m(\Omega)} < \frac{\varepsilon}{2}. \quad (5)$$

Denote $M_j = \max_i \|h_{i,j}(x_i)\|_{H^m(\Omega_i)}$, $j = 1, \dots, p$, and

$$M = \sum_{j=1}^p \left(\binom{d}{1} M_j^{d-1} + \binom{d}{2} M_j^{d-2} + \cdots + \binom{d}{d-1} M_j^1 + 1 \right).$$

Since the universal approximation theorems of FNN [17, 18] can be generalized from $\mathbb{R} \rightarrow \mathbb{R}$ to $\mathbb{R} \rightarrow \mathbb{R}^p$ and $C^m(\Omega_i)$ is dense in $H^m(\Omega_i)$, for $\delta = \min\{1, \frac{\varepsilon}{2M}\}$, there exist FNN structures $\phi_i(x_i; \theta_i)$, $i = 1, \dots, d$, which are defined by (1), such that

$$\|h_{i,j}(x_i) - \phi_{i,j}(x_i; \theta_i)\|_{L^2(\Omega_i)} < \delta, \quad i = 1, \dots, d, \quad j = 1, \dots, p. \quad (6)$$

Denote $e_{i,j}(x_i) = \phi_{i,j}(x_i; \theta_i) - h_{i,j}(x_i)$, inequalities in (6) imply that $\|e_{i,j}(x_i)\|_{H^m(\Omega_i)} < \delta$.

Since the property of multidimensional integrations on the tensor product domain Ω , for any $g_i(x_i) \in H^m(\Omega_i)$, $i = 1, \dots, d$, the following inequality holds

$$\left\| \prod_{i=1}^d g_i(x_i) \right\|_{H^m(\Omega)} \leq \prod_{i=1}^d \|g_i(x_i)\|_{H^m(\Omega_i)}. \quad (7)$$

For the sake of clarity, we give a simple proof for (7) as follows:

$$\begin{aligned} \left\| \prod_{i=1}^d g_i(x_i) \right\|_{H^m(\Omega)}^2 &= \sum_{|\alpha| \leq m} \left\| D^\alpha \left(\prod_{i=1}^d g_i(x_i) \right) \right\|_{L^2(\Omega)}^2 = \sum_{\alpha_1 + \cdots + \alpha_d \leq m} \left\| \prod_{i=1}^d \frac{\partial^{\alpha_i} g_i(x_i)}{\partial x_i^{\alpha_i}} \right\|_{L^2(\Omega_i)}^2 \\ &= \sum_{\alpha_1 + \cdots + \alpha_d \leq m} \prod_{i=1}^d \left\| \frac{\partial^{\alpha_i} g_i(x_i)}{\partial x_i^{\alpha_i}} \right\|_{L^2(\Omega_i)}^2 \leq \prod_{i=1}^d \left(\sum_{\alpha_i \leq m} \left\| \frac{\partial^{\alpha_i} g_i(x_i)}{\partial x_i^{\alpha_i}} \right\|_{L^2(\Omega_i)}^2 \right) \\ &= \prod_{i=1}^d \|g_i(x_i)\|_{H^m(\Omega_i)}^2. \end{aligned}$$

Then from the property of binomial multiplication and inequality (7), we can build a TNN $\Psi(x; \theta)$ by (3) such that the following inequalities hold

$$\begin{aligned}
\|h(x) - \Psi(x; \theta)\|_{H^m(\Omega)} &= \left\| \sum_{j=1}^p \prod_{i=1}^d h_{i,j}(x_i) - \sum_{j=1}^p \prod_{i=1}^d (h_{i,j}(x_i) + e_{i,j}(x_i)) \right\|_{H^m(\Omega)} \\
&\leq \sum_{j=1}^p \left\| \prod_{i=1}^d h_{i,j}(x_i) - \prod_{i=1}^d (h_{i,j}(x_i) + e_{i,j}(x_i)) \right\|_{H^m(\Omega)} \\
&\leq \sum_{j=1}^p \left(\binom{d}{1} M_j^{d-1} \delta^1 + \binom{d}{2} M_j^{d-2} \delta^2 + \cdots + \binom{d}{d} M_j^0 \delta^d \right) \\
&\leq \sum_{j=1}^p \left(\binom{d}{1} M_j^{d-1} + \binom{d}{2} M_j^{d-2} + \cdots + \binom{d}{d-1} M_j^1 + 1 \right) \delta \\
&\leq M \delta < \frac{\varepsilon}{2}.
\end{aligned} \tag{8}$$

Therefore, from (5), (8) and triangle inequality, we have following estimates

$$\begin{aligned}
&\|f(x) - \Psi(x; \theta)\|_{H^m(\Omega)} \\
&\leq \|f(x) - h(x)\|_{H^m(\Omega)} + \|h(x) - \Psi(x; \theta)\|_{H^m(\Omega)} < \frac{\varepsilon}{2} + \frac{\varepsilon}{2} = \varepsilon.
\end{aligned}$$

This is the desired result (4) and the proof is complete. \square

Although there is no general result to give the relationship between the hyperparameter p and error bounds, there are still some estimations of traditional methods that can be used. For example, the sparse grid method and hyperbolic cross approximation method have become widely-used approximation tools for high-dimensional problems [33, 34]. These two methods also assume that the approximation function has the form (3) after replacing each $\phi_{i,j}(x_i; \theta_i)$ by fixed basis functions. Considering a more restrictive smoothness, [9, 10, 22] show that if the target function is in mixed smoothness space $H_{\text{mix}}^{t,\ell}(\Omega)$, there is an approximation space of p basis functions has a dimension independent approximation rate $\mathcal{O}(p^{s-\ell-t})$ under $H^s(\Omega)$ -norm. Our approach, to some extent, adaptively selects p basis functions by optimization process and can analogously derive $p \sim \mathcal{O}(\varepsilon^{-(s-\ell-t)})$ given tolerance ε in the best case with a large enough TNN structure. The explicit upper bound of p for the given tolerance and comprehensive comparison of TNN and traditional methods in approximation efficiency will be studied in our future work.

3 Quadrature scheme for TNN

In this section, we focus on the numerical integration of polynomial composite function of TNN and its derivatives. Our main theorem shows that the application of TNN can bring a significant reduction of the computational complexity for the related numerical integration. For convenience,

we first introduce the following sets of multiple indices

$$\begin{aligned}\mathcal{B} &:= \left\{ \beta = (\beta_1, \dots, \beta_d) \in \mathbb{N}_0^d \mid |\beta| := \sum_{i=1}^d \beta_i \leq m \right\}, \\ \mathcal{A} &:= \left\{ \alpha = (\alpha_\beta)_{\beta \in \mathcal{B}} \in \mathbb{N}_0^{|\mathcal{B}|} \mid |\alpha| := \sum_{\beta \in \mathcal{B}} \alpha_\beta \leq k \right\},\end{aligned}$$

where \mathbb{N}_0 denotes the set of all non-negative integers, m and k are two positive integers, $|\mathcal{B}|$ and $|\mathcal{A}|$ denote the cardinal numbers of \mathcal{B} and \mathcal{A} , respectively.

For example, if $d = 2$ and $m = 1$, the set \mathcal{B} is follows

$$\mathcal{B} = \{(0, 0), (1, 0), (0, 1)\}, \quad (9)$$

which has 3 members. Then \mathcal{A} is a triple-index set. If $k = 2$, the set \mathcal{A} can be described as follows

$$\mathcal{A} = \{(0, 0, 0), (1, 0, 0), (0, 1, 0), (0, 0, 1), (2, 0, 0), (0, 2, 0), (0, 0, 2), (1, 1, 0), (1, 0, 1), (0, 1, 1)\}. \quad (10)$$

Each index in \mathcal{A} corresponds to the member in \mathcal{B} . For example, we can simply take the order for the members in the set \mathcal{B} as that of (9). Then the member $\alpha = (1, 1, 0) \in \mathcal{A}$ indicates that $\alpha_{(0,0)} = 1$, $\alpha_{(1,0)} = 1$ and $\alpha_{(0,1)} = 0$, the member $\alpha = (2, 0, 0) \in \mathcal{A}$ indicates $\alpha_{(0,0)} = 2$, $\alpha_{(1,0)} = 0$ and $\alpha_{(0,1)} = 0$.

In this paper, we focus on the high-dimensional cases where $m \ll d$ and $k \ll d$. Simple calculation leads to the following equations

$$|\mathcal{B}| = \sum_{j=0}^m \binom{j+d-1}{j}, \quad |\mathcal{A}| = \sum_{j=0}^k \binom{j+|\mathcal{B}|-1}{j}.$$

By further estimation, we know that the scales of magnitudes of $|\mathcal{B}|$ and $|\mathcal{A}|$ are $\mathcal{O}((d+m)^m)$ and $\mathcal{O}(((d+m)^m + k)^k)$, respectively.

Here and after, the parameter θ in (3) will be omitted for brevity without confusion. The activation function of TNN needs to be smooth enough such that $\Psi(x)$ has partial derivatives up to order m . Here, we assume $F(x)$ includes the k -degree complete polynomial of d -dimensional TNN and its partial derivatives up to order m that can be expressed as follows

$$F(x) = \sum_{\alpha \in \mathcal{A}} A_\alpha(x) \prod_{\beta \in \mathcal{B}} \left(\frac{\partial^{|\beta|} \Psi(x)}{\partial x_1^{\beta_1} \cdots \partial x_d^{\beta_d}} \right)^{\alpha_\beta}, \quad (11)$$

where the coefficient $A_\alpha(x)$ is given by the following expansion such that the rank of $A_\alpha(x)$ is not greater than q in the tensor product space $L^2(\Omega_1) \otimes \cdots \otimes L^2(\Omega_d)$

$$A_\alpha(x) = \sum_{\ell=1}^q B_{1,\ell,\alpha}(x_1) B_{2,\ell,\alpha}(x_2) \cdots B_{d,\ell,\alpha}(x_d). \quad (12)$$

Here $B_{i,\ell,\alpha}(x_i)$ denotes the one-dimensional function in $L^2(\Omega_i)$ for $i = 1, \dots, d$ and $\ell = 1, \dots, q$. When using neural networks to solve PDEs, we always need to do the high-dimensional integration

$\int_{\Omega} F(x)dx$. If $\Psi(x)$ is a FNN, $\int_{\Omega} F(x)dx$ can only be treated as a direct d -dimensional numerical integration, which requires exponential scale of computational work according to the dimension d . In practical applications, it is well known that the high-dimensional FNN functions can only be integrated by the Monte-Carlo method with a low accuracy. Different from FNN, we will show that the high-dimensional integration $\int_{\Omega} F(x)dx$ for the TNN can be implemented by the normal numerical quadrature with the polynomial scale of computational work with respect to the dimension d . This means that the TNN can cope with the curse of dimensionality in some sense. The key idea to reduce the computational complexity of the numerical integration $\int_{\Omega} F(x)dx$ is that we can decompose the TNN function $F(x)$ into a tensor product structure.

In order to implement the decomposition, for each $\alpha = (\alpha_1, \dots, \alpha_{|\mathcal{B}|}) \in \mathcal{A}$, we give the following definition

$$\mathcal{B}_{\alpha} := \left\{ \beta = (\beta_1, \dots, \beta_d) \in \mathcal{B} \mid \alpha_{\beta} \geq 1 \right\}.$$

For example, when the sets \mathcal{B} and \mathcal{A} are defined by (9) and (10), respectively, the set \mathcal{B}_{α} corresponding to the member $\alpha = (1, 1, 0) \in \mathcal{A}$ in (10) can be described as follows

$$\mathcal{B}_{\alpha} = \left\{ (0, 0), (1, 0) \right\}.$$

By the definition of the index set \mathcal{A} , we can deduce that $|\mathcal{B}_{\alpha}| \leq k$ for any $\alpha \in \mathcal{A}$.

Since $\Psi(x)$ has the TNN structure (3), the cumprod can be further decomposed as

$$\begin{aligned} \prod_{\beta \in \mathcal{B}_{\alpha}} \left(\frac{\partial^{|\beta|} \Psi(x)}{\partial x_1^{\beta_1} \dots \partial x_d^{\beta_d}} \right)^{\alpha_{\beta}} &= \prod_{\beta \in \mathcal{B}_{\alpha}} \left(\frac{\partial^{|\beta|} \sum_{j=1}^p \phi_{1,j}(x_1) \dots \phi_{d,j}(x_d)}{\partial x_1^{\beta_1} \dots \partial x_d^{\beta_d}} \right)^{\alpha_{\beta}} \\ &= \prod_{\beta \in \mathcal{B}_{\alpha}} \left(\sum_{j=1}^p \frac{\partial^{\beta_1} \phi_{1,j}(x_1)}{\partial x_1^{\beta_1}} \dots \frac{\partial^{\beta_d} \phi_{d,j}(x_d)}{\partial x_d^{\beta_d}} \right)^{\alpha_{\beta}} \\ &= \prod_{\beta \in \mathcal{B}_{\alpha}} \sum_{1 \leq j_1, \dots, j_{\alpha_{\beta}} \leq p} \left(\frac{\partial^{\beta_1} \phi_{1,j_1}(x_1)}{\partial x_1^{\beta_1}} \dots \frac{\partial^{\beta_1} \phi_{1,j_{\alpha_{\beta}}}(x_1)}{\partial x_1^{\beta_1}} \right) \dots \left(\frac{\partial^{\beta_d} \phi_{d,j_1}(x_d)}{\partial x_d^{\beta_d}} \dots \frac{\partial^{\beta_d} \phi_{d,j_{\alpha_{\beta}}}(x_d)}{\partial x_d^{\beta_d}} \right) \\ &= \prod_{\beta \in \mathcal{B}_{\alpha}} \sum_{1 \leq j_1, \dots, j_{\alpha_{\beta}} \leq p} \left(\prod_{\ell=1}^{\alpha_{\beta}} \frac{\partial^{\beta_1} \phi_{1,j_{\ell}}(x_1)}{\partial x_1^{\beta_1}} \right) \dots \left(\prod_{\ell=1}^{\alpha_{\beta}} \frac{\partial^{\beta_d} \phi_{d,j_{\ell}}(x_d)}{\partial x_d^{\beta_d}} \right) \\ &= \sum_{\substack{\beta \in \mathcal{B}_{\alpha}, \ell=1, \dots, \alpha_{\beta}, \\ 1 \leq j_{\beta}, \ell \leq p}} \left(\prod_{\beta \in \mathcal{B}_{\alpha}} \prod_{\ell=1}^{\alpha_{\beta}} \frac{\partial^{\beta_1} \phi_{1,j_{\beta},\ell}(x_1)}{\partial x_1^{\beta_1}} \right) \dots \left(\prod_{\beta \in \mathcal{B}_{\alpha}} \prod_{\ell=1}^{\alpha_{\beta}} \frac{\partial^{\beta_d} \phi_{d,j_{\beta},\ell}(x_d)}{\partial x_d^{\beta_d}} \right). \end{aligned} \quad (13)$$

With the help of expansion (13), we can give the following expansion for $F(x)$

$$F(x) = \sum_{\alpha \in \mathcal{A}} \left(\sum_{\ell=1}^q B_{1,\ell,\alpha}(x_1) \dots B_{d,\ell,\alpha}(x_d) \right)$$

$$\begin{aligned}
& \sum_{\substack{\beta \in \mathcal{B}_\alpha, \ell=1, \dots, \alpha_\beta, \\ 1 \leq j_\beta, \ell \leq p}} \left(\prod_{\beta \in \mathcal{B}_\alpha} \prod_{\ell=1}^{\alpha_\beta} \frac{\partial^{\beta_1} \phi_{1,j_\beta, \ell}(x_1)}{\partial x_1^{\beta_1}} \right) \cdots \left(\prod_{\beta \in \mathcal{B}_\alpha} \prod_{\ell=1}^{\alpha_\beta} \frac{\partial^{\beta_d} \phi_{d,j_\beta, \ell}(x_d)}{\partial x_d^{\beta_d}} \right) \\
&= \sum_{\alpha \in \mathcal{A}} \sum_{\ell=1}^q \sum_{\substack{\beta \in \mathcal{B}_\alpha, \ell=1, \dots, \alpha_\beta, \\ 1 \leq j_\beta, \ell \leq p}} \left(B_{1,\ell,\alpha}(x_1) \prod_{\beta \in \mathcal{B}_\alpha} \prod_{\ell=1}^{\alpha_\beta} \frac{\partial^{\beta_1} \phi_{1,j_\beta, \ell}(x_1)}{\partial x_1^{\beta_1}} \right) \\
&\quad \cdots \left(B_{d,\ell,\alpha}(x_d) \prod_{\beta \in \mathcal{B}_\alpha} \prod_{\ell=1}^{\alpha_\beta} \frac{\partial^{\beta_d} \phi_{d,j_\beta, \ell}(x_d)}{\partial x_d^{\beta_d}} \right). \tag{14}
\end{aligned}$$

Based on the decomposition (14), we have the following splitting scheme for the integration $\int_\Omega F(x)dx$

$$\begin{aligned}
\int_\Omega F(x)dx &= \sum_{\alpha \in \mathcal{A}} \sum_{\ell=1}^q \sum_{\substack{\beta \in \mathcal{B}_\alpha, \ell=1, \dots, \alpha_\beta, \\ 1 \leq j_\beta, \ell \leq p}} \int_{\Omega_1} \left(B_{1,\ell,\alpha}(x_1) \prod_{\beta \in \mathcal{B}_\alpha} \prod_{\ell=1}^{\alpha_\beta} \frac{\partial^{\beta_1} \phi_{1,j_\beta, \ell}(x_1)}{\partial x_1^{\beta_1}} \right) dx_1 \\
&\quad \cdots \int_{\Omega_d} \left(B_{d,\ell,\alpha}(x_d) \prod_{\beta \in \mathcal{B}_\alpha} \prod_{\ell=1}^{\alpha_\beta} \frac{\partial^{\beta_d} \phi_{d,j_\beta, \ell}(x_d)}{\partial x_d^{\beta_d}} \right) dx_n. \tag{15}
\end{aligned}$$

Now, we come to introduce the detailed numerical integration method for the TNN function $F(x)$. Without loss of generality, for $i = 1, \dots, d$, we choose N_i Gauss points $\{x_i^{(n_i)}\}_{n_i=1}^{N_i}$ and the corresponding weights $\{w_i^{(n_i)}\}_{n_i=1}^{N_i}$ for the i -th dimensional domain Ω_i , and denote $N = \max\{N_1, \dots, N_d\}$ and $\underline{N} = \min\{N_1, \dots, N_d\}$. Introducing the index $n = (n_1, \dots, n_d) \in \mathcal{N} := \{1, \dots, N_1\} \times \dots \times \{1, \dots, N_d\}$, then the Gauss points and their corresponding weights for the integration (15) can be expressed as follows

$$\begin{aligned}
\{x^{(n)}\}_{n \in \mathcal{N}} &= \left\{ \{x_1^{(n_1)}\}_{n_1=1}^{N_1}, \{x_2^{(n_2)}\}_{n_2=1}^{N_2}, \dots, \{x_d^{(n_d)}\}_{n_d=1}^{N_d} \right\}, \\
\{w^{(n)}\}_{n \in \mathcal{N}} &= \left\{ \{w_1^{(n_1)}\}_{n_1=1}^{N_1} \times \{w_2^{(n_2)}\}_{n_2=1}^{N_2} \times \dots \times \{w_d^{(n_d)}\}_{n_d=1}^{N_d} \right\}. \tag{16}
\end{aligned}$$

Then from (11) and (12), the numerical integration $\int_\Omega F(x)dx$ can be computed as follows:

$$\int_\Omega F(x)dx \approx \sum_{n \in \mathcal{N}} w^{(n)} \sum_{\alpha \in \mathcal{A}} \left(\sum_{\ell=1}^q B_{1,\ell,\alpha}(x_1^{(n_1)}) \cdots B_{d,\ell,\alpha}(x_d^{(n_d)}) \right) \prod_{\beta \in \mathcal{B}_\alpha} \left(\frac{\partial^{|\beta|} \Psi(x^{(n)})}{\partial x_1^{\beta_1} \cdots \partial x_d^{\beta_d}} \right)^{\alpha_\beta}. \tag{17}$$

Fortunately, with the help of expansions (13) and (15), we can give the following splitting numerical integration scheme for $\int_\Omega F(x)dx$:

$$\begin{aligned}
\int_\Omega F(x)dx &\approx \sum_{\alpha \in \mathcal{A}} \sum_{\ell=1}^q \sum_{\substack{\beta \in \mathcal{B}_\alpha, \ell=1, \dots, \alpha_\beta, \\ 1 \leq j_\beta, \ell \leq p}} \left(\sum_{n_1=1}^{N_1} w_1^{(n_1)} B_{1,\ell,\alpha}(x_1^{(n_1)}) \prod_{\beta \in \mathcal{B}_\alpha} \prod_{\ell=1}^{\alpha_\beta} \frac{\partial^{\beta_1} \phi_{1,j_\beta, \ell}(x_1^{(n_1)})}{\partial x_1^{\beta_1}} \right) \\
&\quad \cdots \left(\sum_{n_d=1}^{N_d} w_d^{(n_d)} B_{d,\ell,\alpha}(x_d^{(n_d)}) \prod_{\beta \in \mathcal{B}_\alpha} \prod_{\ell=1}^{\alpha_\beta} \frac{\partial^{\beta_d} \phi_{d,j_\beta, \ell}(x_d^{(n_d)})}{\partial x_d^{\beta_d}} \right). \tag{18}
\end{aligned}$$

The quadrature scheme (18) decomposes the high-dimensional integration $\int_{\Omega} F(x)dx$ into to a series of 1-dimensional integration, which is the main contribution of this paper. Due to the simplicity of the 1-dimensional integration, the scheme (18) can reduce the computational work of the high-dimensional integration for the d -dimensional function $F(x)$ to the polynomial scale of dimension d . Theorem 2 gives the corresponding result.

Theorem 2. *Assume that the function $F(x)$ is defined as (11), where the coefficient $A_{\alpha}(x)$ has the expansion (12). Employ Gauss quadrature points and corresponding weights (16) to $F(x)$ on the d -dimensional tensor product domain Ω . If the function $\Psi(x)$ involved in the function $F(x)$ has TNN form (3), the efficient quadrature scheme (18) is equivalent to (17) and has $2\underline{N}$ -th order accuracy. Let T_1 denote the computational complexity for the 1-dimensional function evaluation operations. The computational complexity can be bounded by $\mathcal{O}(dqT_1k^2p^k((d+m)^m+k)^kN)$, which is the polynomial scale of the dimension d .*

Proof. First, we point out that the number of $j_{\beta,\ell}$ in the last summation of (13) is no more than k . This result can be easily proved by the following inequality

$$\sum_{\beta \in \mathcal{B}_{\alpha}} \alpha_{\beta} = |\alpha| \leq k.$$

Then, by direct calculation, the computational complexity of (18) can be bounded by $\mathcal{O}(dqT_1k^2p^k((d+m)^m+k)^kN)$. Since the 1-dimensional integration with N_i Gauss points has $2N_i$ -th order accuracy and the equivalence of (18) and (17), both quadrature schemes (18) and (17) have the $2\underline{N}$ -th order accuracy. Then the proof is complete. \square

Remark 1. *Theorem 2 considers using 1-dimensional Gauss points to compute d -dimensional integrations. Other types of 1-dimensional quadrature schemes can also be employed to do the d -dimensional integration and have similar results. In numerical examples, we decompose each Ω_i into subintervals with mesh size h and choose N_i 1-dimensional Gauss points in each subinterval. Then the deduced d -dimensional quadrature scheme has accuracy $\mathcal{O}(h^{2\underline{N}}/(2\underline{N})!)$, where the included constant depends on the smoothness of $F(x)$.*

If $\Psi(x)$ does not have the tensor form, for example, $\Psi(x)$ is a d -dimensional FNN and use the same quadrature scheme (18), the computational complexity is $\mathcal{O}((dqT_1+kT_d)((d+m)^m+k)^kN^d)$, where T_d denotes the complexity of the d -dimensional function evaluation operations.

4 Solving high-dimensional eigenvalue problem by TNN

This section is devoted to discussing the applications of TNNs to the numerical solution of the high-dimensional second order elliptic eigenvalue problems. For simplicity, we are concerned with the following model problem:

$$\begin{cases} -\Delta u + vu = \lambda u, & \text{in } \Omega, \\ u = 0, & \text{on } \partial\Omega, \end{cases} \quad (19)$$

where $\Omega = \Omega_1 \times \cdots \times \Omega_d$, each $\Omega_i = (a_i, b_i)$, $i = 1, \dots, d$ is a bounded interval in \mathbb{R} , $v \in L^2(\Omega)$ is a potential function. We assume that the rank of v is finite in the tensor product space $L^2(\Omega_1) \otimes \cdots \otimes L^2(\Omega_d)$. The potential function v often occurs in quantum mechanics problems. In this paper, we consider the following cases:

zero function

$$v(x) = 0, \quad \text{in } \Omega, \quad (20)$$

harmonic oscillator

$$v(x) = \sum_{i=1}^d x_i^2, \quad \text{in } \Omega, \quad (21)$$

and coupled oscillator

$$v(x) = \sum_{i=1}^d x_i^2 - \sum_{i=1}^{d-1} x_i x_{i+1}, \quad (22)$$

and the Column potential for Schrödinger equation.

In quantum mechanics, the eigenvalue problem (19) with the potential function (20) is the Schrödinger equation with infinite potential well. The eigenvalue problem with the potential (21) comes from the truncation of the Schrödinger equation with the harmonic oscillator potential which is defined in the whole space. The more complicated eigenvalue problem with the potential (22) describes the system of chains of d coupled harmonic oscillators which is described in detail in [3].

There is a well-known variational principle or minimum theorem of the eigenvalue problem (19) for the smallest eigenpair (λ, u) :

$$\lambda = \min_{w \in H_0^1(\Omega)} \mathcal{R}(w) = \min_{w \in H_0^1(\Omega)} \frac{\int_{\Omega} |\nabla w|^2 dx + \int_{\Omega} v w^2 dx}{\int_{\Omega} w^2 dx}, \quad (23)$$

where $\mathcal{R}(w)$ denotes the Rayleigh quotient for the function $w \in H_0^1(\Omega)$.

In order to solve the eigenvalue problem (19), we build a TNN structure $\Psi(x; \theta)$ which is defined by (3), and denote the set of all possible values of θ as Θ . In order to avoid the penalty on boundary condition, we simply use the method in [11] to treat the Dirichlet boundary condition. This method is firstly proposed in [24, 25]. For $i = 1, \dots, d$, the i -th subnetwork $\phi_i(x_i; \theta_i)$ is defined as follows:

$$\begin{aligned} \phi_i(x_i; \theta_i) &:= (x_i - a_i)(b_i - x_i) \hat{\phi}_i(x_i; \theta_i) \\ &= ((x_i - a_i)(b_i - x_i) \hat{\phi}_{i,1}(x_i; \theta_i), \dots, (x_i - a_i)(b_i - x_i) \hat{\phi}_{i,p}(x_i; \theta_i))^T, \end{aligned}$$

where $\hat{\phi}_i(x_i; \theta_i)$ is a FNN from \mathbb{R} to \mathbb{R}^p with sufficient smooth activation functions, such that $\Psi(x; \theta) \in H_0^1(\Omega)$.

The trial function set V is modeled by the TNN structure $\Psi(x; \theta)$ where parameters θ take all the possible values and it is obvious that $V \subset H_0^1(\Omega)$. The solution and the parameters $(\lambda^*, \Psi(x; \theta^*))$ of the following optimization problem are approximations to the smallest eigenpair:

$$\lambda^* = \min_{\Psi(x; \theta) \in V} \mathcal{R}(\Psi(x; \theta)) = \min_{\theta \in \Theta} \frac{\int_{\Omega} |\nabla \Psi(x; \theta)|^2 dx + \int_{\Omega} v(x) \Psi^2(x; \theta) dx}{\int_{\Omega} \Psi^2(x; \theta) dx} = \mathcal{R}(\Psi(x; \theta^*)). \quad (24)$$

Note that all integrands of the numerator and the denominator of (24) have the form (11). With the help of Theorem 2, we can implement these numerical integrations by scheme (18) with the computational work being bounded by the polynomial scale of dimension d . We choose Gauss points and their corresponding weights which are defined by (16) to compute these integrations, and define the loss function as follows:

$$L(\theta) := \frac{\sum_{n \in \mathcal{N}} w^{(n)} |\nabla \Psi(x^{(n)}, \theta)|^2 + \sum_{n \in \mathcal{N}} w^{(n)} v(x^{(n)}) \Psi^2(x^{(n)}; \theta)}{\sum_{n \in \mathcal{N}} \Psi^2(x^{(n)}; \theta)}. \quad (25)$$

In this paper, the gradient descent (GD) method is adopted to minimize the loss function $L(\theta)$. The GD scheme can be described as follows:

$$\theta^{(k+1)} = \theta^{(k)} - \eta \nabla L(\theta^{(k)}), \quad (26)$$

where $\theta^{(k)}$ denotes the parameters after the k -th GD step, η is the learning rate (step size).

Different from the general FNN-based machine learning method, we use the fixed quadrature points $\{x^{(n)}\}_{n \in \mathcal{N}}$ to do the numerical integration in this paper. Using the fixed quadrature points for FNN, the computational work for the numerical integration will depend exponentially on the dimension d . In order to avoid the “curse of dimensionality”, in the numerical implementation for solving high-dimensional PDEs by FNN-based method, the stochastic gradient descent (SGD) method [21] with Monte-Carlo integration are always used [6]. The application of random sampling quadrature points always leads to the low accuracy and instability convergence for the FNN method.

Fortunately, based on TNN structure in the loss function (25), Theorem 2 shows that the numerical integration does not encounter “curse of dimensionality” since the computational work can be bounded by the polynomial scale of dimension d . This is the reason we can use GD method to solve the optimization problem (24) instead of SGD in this paper. That is to say, using all quadrature points to implement the integration and the GD step (26) in TNN-based machine learning are reasonable. With the help of the high accuracy of the tensor product with Gauss points and Theorem 1, the high accuracy of the TNN-based method can be guaranteed.

Although in this paper, we simply choose a fixed rank p in our numerical examples, it is worth mentioning that, by adding columns to the weight matrices of the output layer in each subnetwork, we can transfer weights from the old TNN to the new one to improve the rank p . We can stop this process when the accuracy improvement is small enough. Choosing the rank p by the computable posterior error estimation and the corresponding transfer learning framework will be presented in our future work.

Remark 2. *In this section, we are mainly talking about solving high-dimensional eigenvalue problems by TNN. It is worth mentioning that TNN structure can be applied naturally to solve PDEs with different types of loss functions. We will do a preliminary test in our numerical examples.*

5 Numerical examples

In this section, we provide several examples to validate the efficiency and accuracy of the TNN-based machine learning method proposed in this paper. The first two examples are used to demonstrate

the high accuracy of the TNN method for high-dimensional problems. We will explore the effect of the vital hyperparameter p on the accuracy in the third example where the ground state energy may not be exactly represented by a finite-rank CP decomposition. The fourth example for the ground state of a helium atom which comes from the real physical problem is used to give an illuminating way to deal with the problem that does not satisfy the assumption (12). Note that in the fourth example, the potential cannot be exactly expressed as a CP decomposition of finite rank, this makes the loss function no longer satisfy the assumption (12). In the last example, we solve a boundary value problem with Neumann boundary condition to show the efficiency of TNN for solving high-dimensional PDEs.

In order to show the convergence behavior and accuracy of eigenfunction approximations by TNN, we define the $L^2(\Omega)$ projection operator $\mathcal{P} : H_0^1(\Omega) \rightarrow \text{span}\{\Psi(x; \theta^*)\}$ as follows:

$$\langle \mathcal{P}u, v \rangle_{L^2} = \langle u, v \rangle_{L^2} := \int_{\Omega} uv dx, \quad \forall v \in \text{span}\{\Psi(x; \theta^*)\} \text{ for } u \in H_0^1(\Omega).$$

And we define the $H^1(\Omega)$ projection operator $\mathcal{Q} : H_0^1(\Omega) \rightarrow \text{span}\{\Psi(x; \theta^*)\}$ as follows:

$$\langle \mathcal{Q}u, v \rangle_{H^1} = \langle u, v \rangle_{H^1} := \int_{\Omega} \nabla u \cdot \nabla v dx, \quad \forall v \in \text{span}\{\Psi(x; \theta^*)\} \text{ for } u \in H_0^1(\Omega).$$

Then we define the following errors for the approximated eigenvalue λ^* and eigenfunction $\Psi(x; \theta^*)$

$$e_{\lambda} := \frac{|\lambda^* - \lambda|}{|\lambda|}, \quad e_{L^2} := \frac{\|u - \mathcal{P}u\|_{L^2(\Omega)}}{\|u\|_{L^2(\Omega)}}, \quad e_{H^1} := \frac{|u - \mathcal{Q}u|_{H^1(\Omega)}}{|u|_{H^1(\Omega)}},$$

in all eigenvalue examples. As for Neumann boundary value problem, we define the following errors for the approximated solution $\Psi(x; \theta^*)$

$$\widehat{e}_{L^2} := \frac{\|u - \Psi(x; \theta^*)\|_{L^2(\Omega)}}{\|f\|_{L^2(\Omega)}}, \quad \widehat{e}_{H^1} := \frac{|u - \Psi(x; \theta^*)|_{H^1(\Omega)}}{|f|_{H^1(\Omega)}}.$$

Here $\|\cdot\|_{L^2}$ and $|\cdot|_{H^1}$ denote $L^2(\Omega)$ norm and $H^1(\Omega)$ seminorm, respectively. These relative errors are often used to test numerical methods for eigenvalue problems and PDEs. We use the quadrature scheme (18) to compute e_{L^2} and e_{H^1} with the same Gauss points and weights as computing the loss functions if the rank of the exact solution $u(x)$ is finite in the tensor product space $L^2(\Omega_1) \otimes \cdots \otimes L^2(\Omega_d)$, otherwise we only report e_{λ} . With the help of Theorem 2 and Gauss quadrature points, the high efficiency and accuracy for computing e_{L^2} and e_{H^1} can be guaranteed.

In implementation, we train the networks by Adam optimizer [21] and use automatic differentiation for derivatives in PyTorch.

5.1 Laplace eigenvalue problem

In the first example, the potential function is defined as (20) with the computational domain $\Omega = [0, 1]^d$. Then the exact smallest eigenvalue and eigenfunction are

$$\lambda = d\pi^2, \quad u(x) = \prod_{i=1}^d \sin(\pi x_i).$$

First, we test high-dimensional cases with $d = 5, 10, 20$, respectively. Quadrature scheme for TNN is obtained by decomposing each Ω_i ($i = 1, \dots, d$) into 10 equal subintervals and choosing 16 Gauss points on each subinterval. The Adam optimizer is employed with a learning rate of 0.003 to train the TNN with rank $p = 10$ depth 2 and width 50 in each dimension. Figure 3 shows the relative errors e_λ , e_{L^2} and e_{H^1} versus the number of epochs. The final relative errors after 100000 epochs are reported in Table 1 for different dimensional cases. Then we can find that the TNN method has almost the same convergence behaviors for different dimensions.

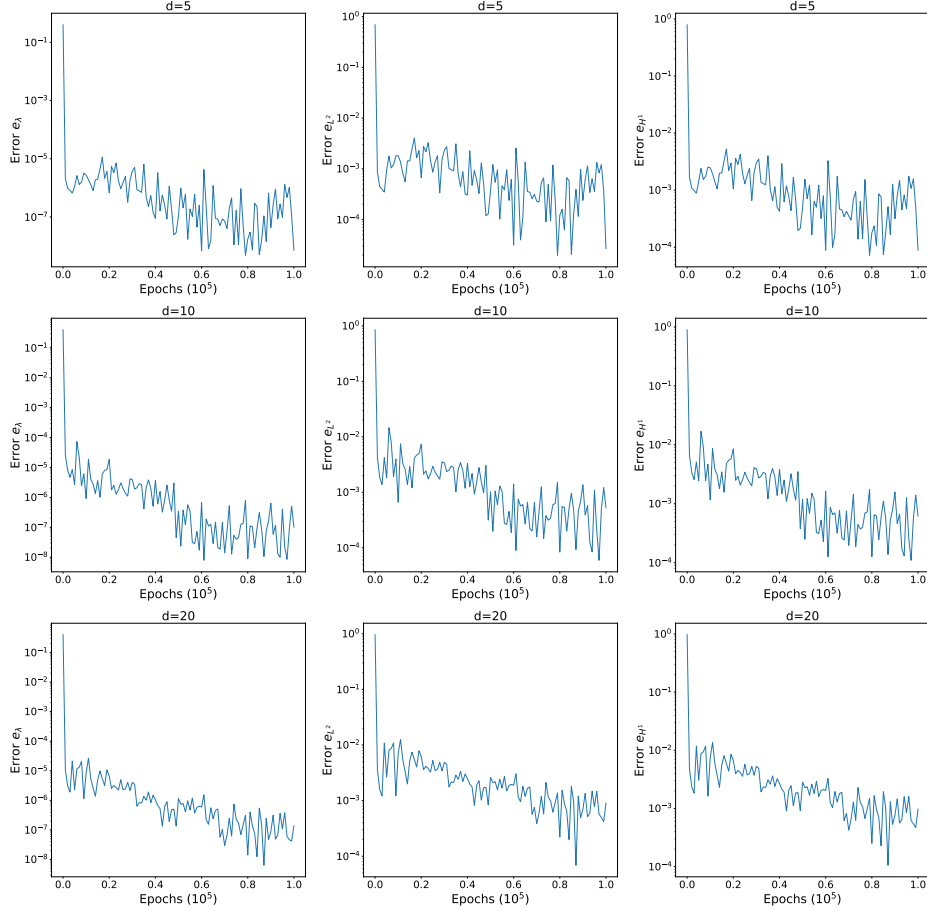


Figure 3: Relative errors during the training process for Laplace eigenvalue problem: for $d = 5, 10$, and 20 . The left column shows the relative errors of eigenvalue approximations, the middle column shows the relative $L^2(\Omega)$ errors and the right column shows the relative $H^1(\Omega)$ errors of eigenfunction approximations.

Since the definition of TNN (3) and the form of the loss function (23), multiplying by a scale does not mathematically affect the final result of the optimization problem.

To improve the numerical stability, we decompose each Ω_i ($i = 1, \dots, d$) into 10 equal subintervals and choose 4 Gauss points on each subinterval. The Adam optimizer is employed with a smaller learning rate of 0.0001 to train a smaller scale TNN with rank $p = 10$ depth 2 and width 20 in each dimension. Results after 50000 epochs are shown in Figure 4 and Table 2. In

Table 1: Errors of Laplace eigenvalue problem for $d = 5, 10, 20$.

d	e_λ	e_{L^2}	e_{H^1}
5	4.838e-09	1.977e-05	7.231e-05
10	7.916e-09	8.941e-05	1.261e-04
20	6.354e-09	6.872e-05	1.052e-04

ultra-high-dimensional cases, the TNN method still has almost the same convergence behaviors for different dimensions and the final results are not much worse than that in high-dimensional cases. All relative errors are on a convincing order of magnitude.

Table 2: Errors of Laplace eigenvalue problem for $d = 128, 256, 512$.

d	e_λ	e_{L^2}	e_{H^1}
128	1.674e-07	1.041e-03	1.118e-03
256	1.497e-07	1.484e-03	1.534e-03
512	1.629e-07	2.500e-03	2.532e-03

5.2 Eigenvalue problem with harmonic oscillator

In the second example, the potential function is defined as (21). Then the exact smallest eigenvalue and eigenfunction are

$$\lambda = d, \quad u(x) = \prod_{i=1}^d e^{-x_i^2/2}.$$

Then we test ultra-high-dimensional cases with $d = 128, 256, 512$, respectively. Although the usual problem doesn't have such a high dimension, it is important to point out that since the TNN structure (3) includes the compound of d terms, in ultra-high-dimensional cases, numerical instability may occur. To avoid this problem, we do a suitable scale for each dimension of TNN at the initialization step. As the first example in Section 5.1, high-dimensional cases with $d = 5, 10, 20$ and ultra-high-dimensional cases with $d = 128, 256, 512$ are also tested, respectively. We truncate the computational domain from \mathbb{R}^d to $[-5, 5]^d$, use 100 equal subintervals and 16 Gauss points quadrature scheme for the cases of $d = 5, 10, 20$, and 50 equal subintervals and 4 Gauss points quadrature scheme for $d = 128, 256, 512$. The Adam optimizer is employed to train TNN of the same size as the first example but with a bigger learning rate of 0.01 and 0.001 for high-dimensional cases and ultra-high-dimensional cases, respectively. Numerical results for $d = 5, 10, 20$ are shown in Figure 5 and Table 3 and that for $d = 128, 256, 512$ are shown in Figure 6 and Table 4. Since we truncate the computational domain, it is reasonable that the final relative errors are a little worse

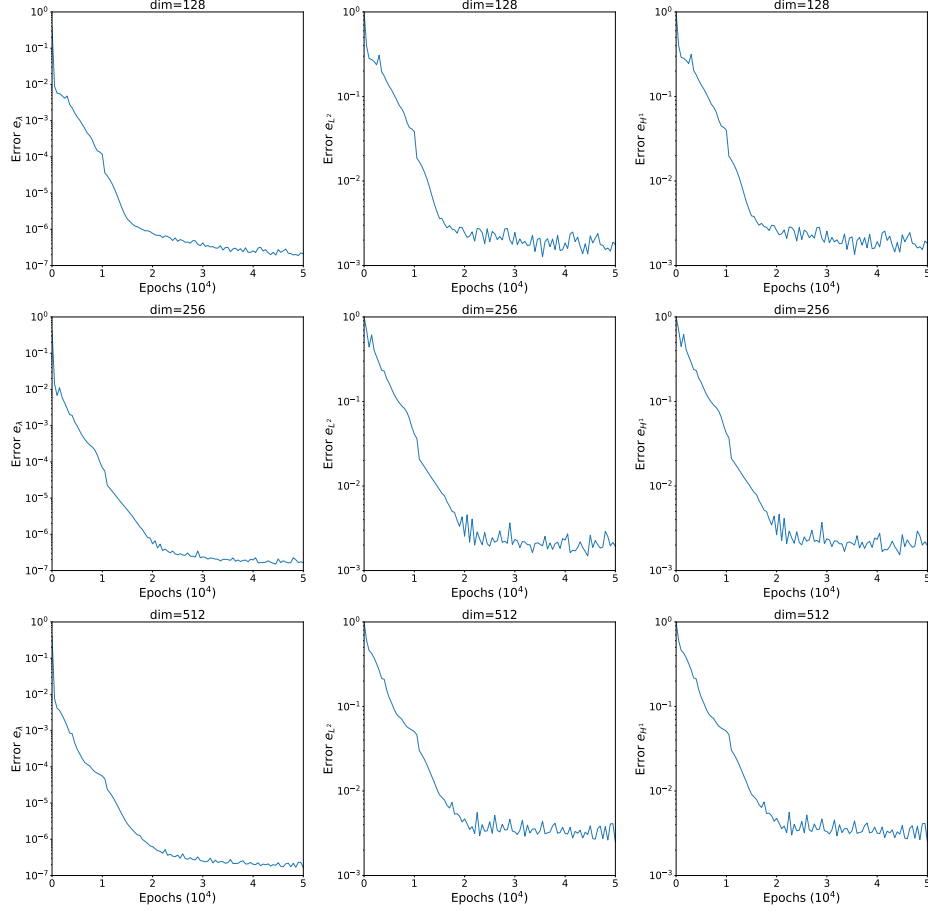


Figure 4: Relative errors during the training process for Laplace eigenvalue problem: for $d = 128$, 256 and 512. The left column shows the relative errors of eigenvalue approximations, the middle column shows the relative $L^2(\Omega)$ errors and the right column shows the relative $H^1(\Omega)$ errors of eigenfunction approximations.

than the examples of the Laplace eigenvalue problem. There should exist some room for improving the accuracy.

Table 3: Errors of the harmonic oscillator problem for $d = 5, 10, 20$.

d	e_λ	e_{L^2}	e_{H^1}
5	4.241e-07	3.626e-04	8.431e-04
10	2.446e-07	2.709e-04	6.889e-04
20	7.225e-07	1.361e-03	1.555e-03

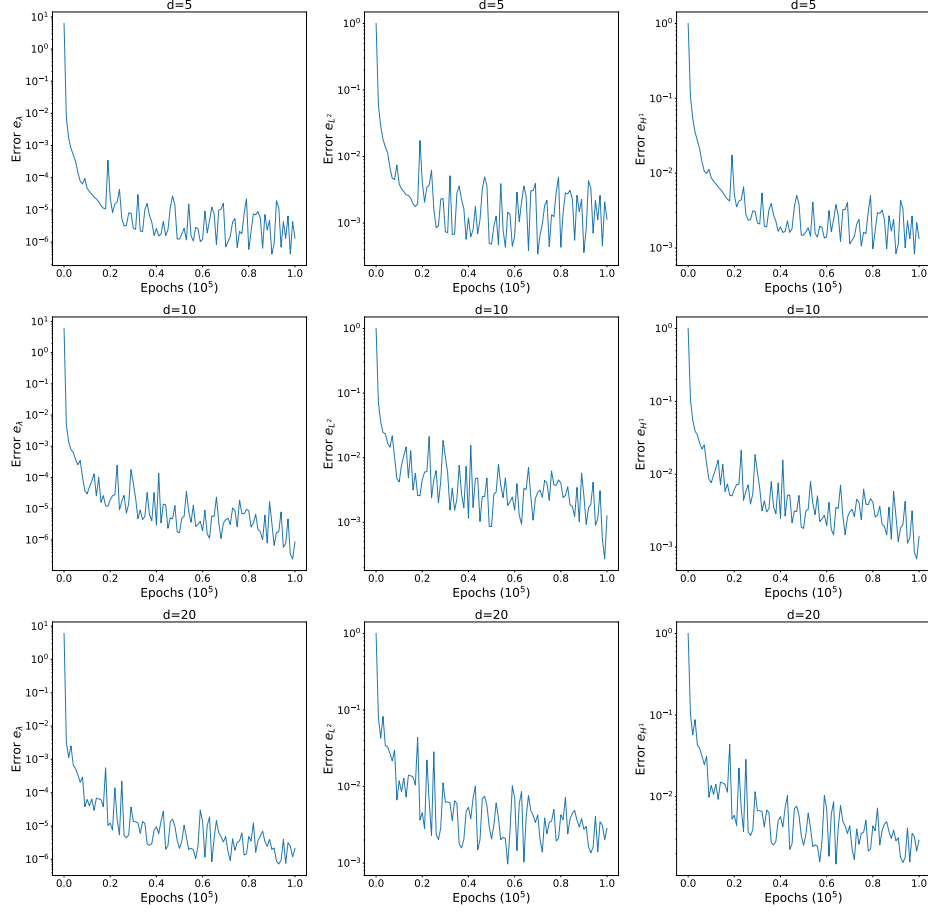


Figure 5: Relative errors during the training process for the harmonic oscillator problem: for $d = 5, 10, 20$. The left column shows the relative errors of eigenvalue, the middle column shows the relative L^2 errors and the right column shows the relative H^1 errors of eigenfunction approximations.

Table 4: Errors of the harmonic oscillator problem for $d = 128, 256, 512$.

d	e_λ	e_{L^2}	e_{H^1}
128	5.483e-06	8.221e-03	8.500e-03
256	7.166e-06	1.362e-02	1.387e-02
512	8.530e-06	2.471e-02	2.480e-02

5.3 Eigenvalue problem with coupled harmonic oscillator

In the third example, the potential function is defined as (22). Similar to the derivation in [3], the exact smallest eigenvalue is

$$\lambda_0 = \sum_{i=1}^d \sqrt{1 - \cos\left(\frac{i\pi}{d+1}\right)},$$

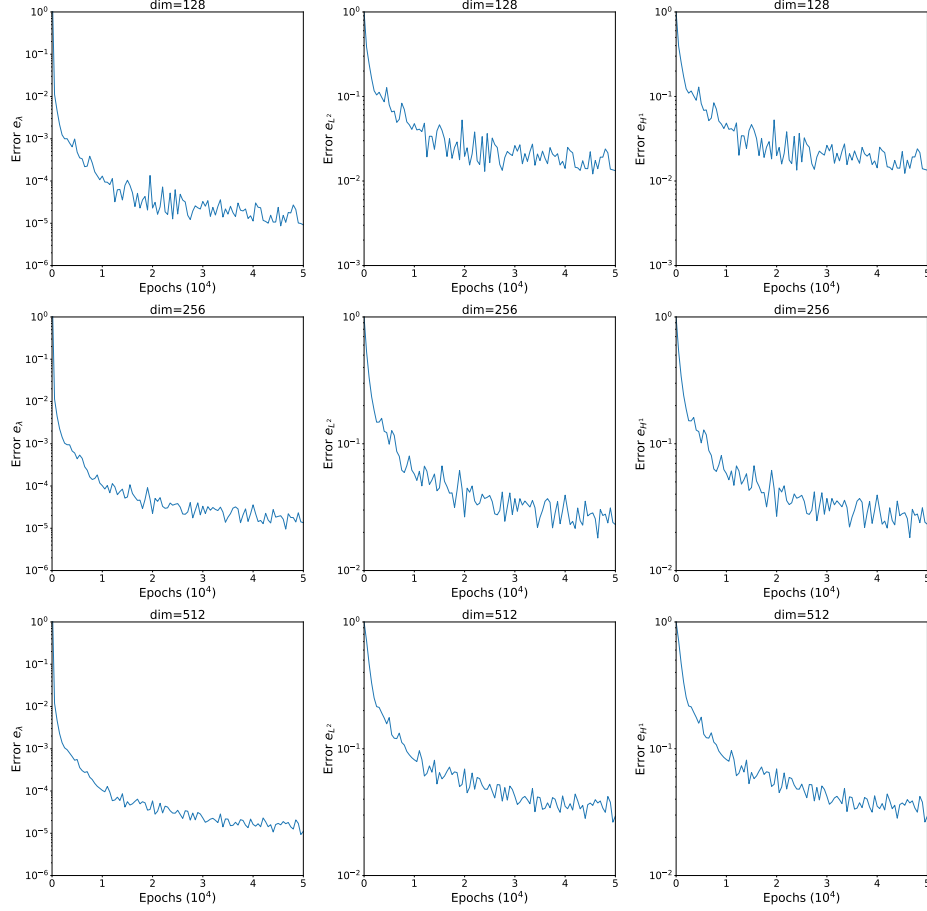


Figure 6: Relative errors during the training process for the harmonic oscillator problem: for $d = 128, 256, 512$. The left column shows the relative errors of eigenvalue approximations, the middle column shows the relative L^2 errors and the right column shows the relative H^1 errors of eigenfunction approximations.

and the exact eigenfunction has Gaussian form. In this example, we test the case of $d = 4$. Then the exact eigenfunction is

$$\begin{aligned}
& u(x_1, x_2, x_3, x_4) \\
&= \exp \left[-\frac{1}{2}(\omega_1 a^2 + \omega_2 b^2 + \omega_3 a^2 + \omega_4 b^2)(x_1^2 + x_3^2) - \frac{1}{2}(\omega_1 b^2 + \omega_2 a^2 + \omega_3 b^2 + \omega_4 a^2)(x_2^2 + x_4^2) \right. \\
&\quad - ab(-\omega_1 - \omega_2 + \omega_3 + \omega_4)(x_1 x_2 + x_3 x_4) - ab(\omega_1 - \omega_2 + \omega_3 - \omega_4)(x_1 x_4 + x_2 x_3) \\
&\quad \left. - (-\omega_1 a^2 + \omega_2 b^2 + \omega_3 a^2 - \omega_4 b^2)x_1 x_3 - (-\omega_1 b^2 + \omega_2 a^2 + \omega_3 b^2 - \omega_4 a^2)x_2 x_4 \right],
\end{aligned}$$

where $a = \sqrt{5 - \sqrt{5}}/(2\sqrt{5})$, $b = \sqrt{5 + \sqrt{5}}/(2\sqrt{5})$, $\omega_1 = \sqrt{5 + \sqrt{5}}/2$, $\omega_2 = \sqrt{3 + \sqrt{5}}/2$, $\omega_3 = \sqrt{5 - \sqrt{5}}/2$, $\omega_4 = \sqrt{3 - \sqrt{5}}/2$. To demonstrate the efficiency of the proposed method, we take hyperparameter p from 1 to 30 and train the TNN with depth 2 and width 50 in each dimension to investigate the dependence of the convergence behavior on the rank p . We train all the cases by the Adam optimizer with the same learning rate of 0.001 and epochs of 500000. The computational

domain is truncated to $[-5, 5]^d$. And we decompose the interval $[-5, 5]$ in each dimensional into 100 equal subintervals and choose 16 Gauss points on each subinterval. The relative errors e_λ during the training process for different p are shown in Figure 7 and Figure 8 demonstrates how the final error changes as p increases. From Figures 7 and 8, we can find that the proposed method converges at an impressive accuracy.

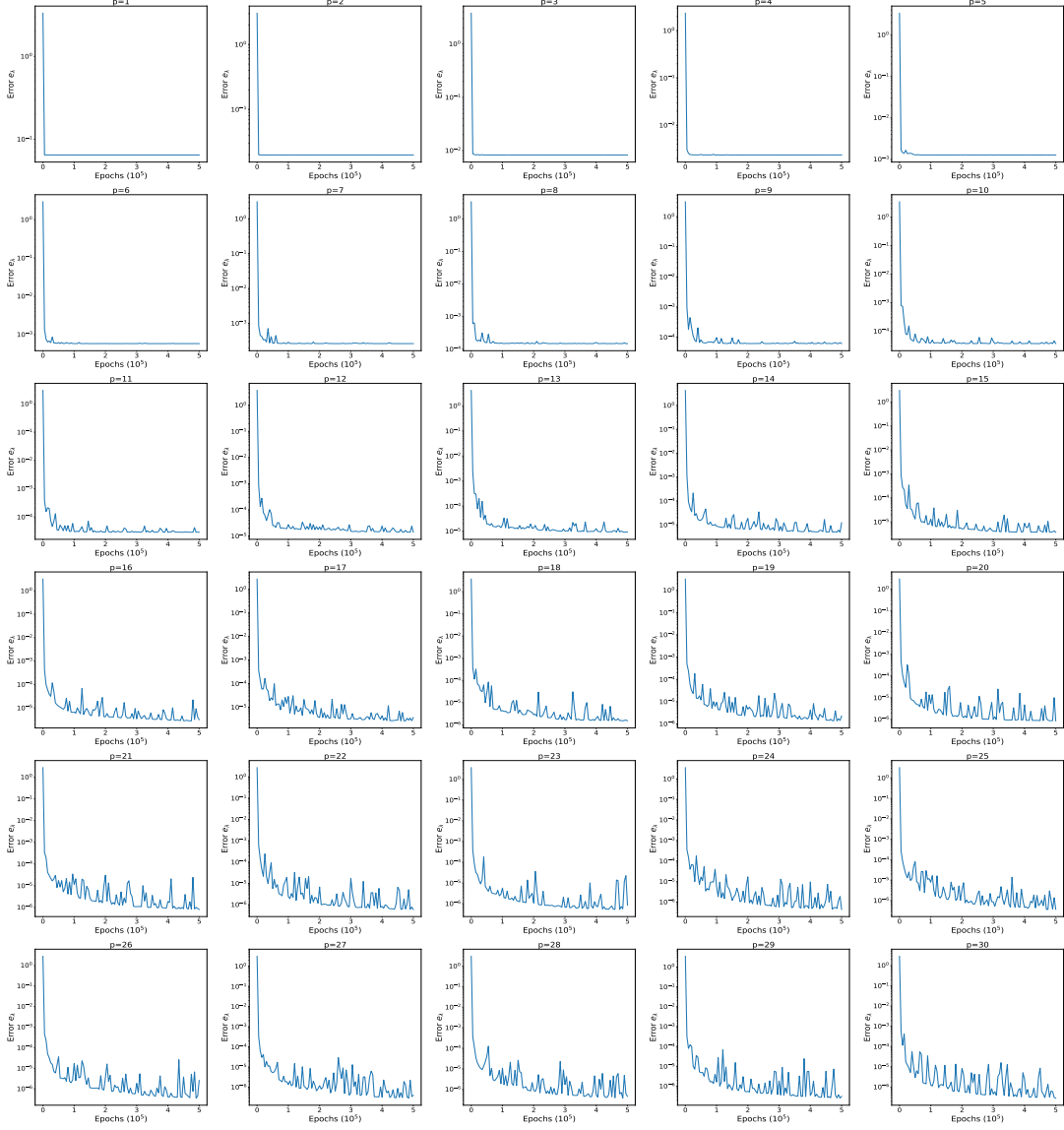


Figure 7: Relative errors during the training process for the coupled harmonic oscillator: the rank p increases from 1 to 30.

5.4 Ground state of helium atom

In the fourth example, we consider the Schrödinger equation of the helium atom whose potential cannot be exactly expressed as a CP decomposition of finite rank. The wave function of the helium

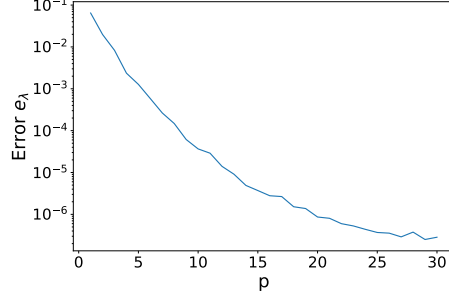


Figure 8: Relative errors e_λ versus hyperparameter p for the coupled harmonic oscillator ($d = 4$).

atom with the fixed nucleus in Euclidean coordinates $\Psi(x_1, y_1, z_1, x_2, y_2, z_2)$ satisfies the following eigenvalue problem

$$-\frac{1}{2}\Delta\Psi - \frac{2\Psi}{r_1} - \frac{2\Psi}{r_2} + \frac{\Psi}{r_{12}} = E\Psi, \quad (27)$$

where

$$\begin{aligned} r_1^2 &= x_1^2 + y_1^2 + z_1^2, & r_2^2 &= x_2^2 + y_2^2 + z_2^2, \\ r_{12}^2 &= (x_1 - x_2)^2 + (y_1 - y_2)^2 + (z_1 - z_2)^2. \end{aligned}$$

Since the potential term $\frac{1}{r_{12}}$ in (27) can not be expressed as a CP decomposition of finite rank in either Euclidean or spherical coordinates, it is impossible to give the analytical expressions for exact energy E and wave function Ψ and it is also difficult to perform the TNN-based machine learning directly on this potential. Fortunately, Hylleraas [19] chose the three independent variables r_1, r_2, θ , with θ being the angle between r_1 and r_2 , to determine the form and the size of a triangle that is composed of the nucleus and two electrons. The coordinates $\{r_1, r_2, \theta\}$ are enough to describe the wave function for the ground state of the helium atom and the corresponding wave function $\Psi(r_1, r_2, \theta)$ satisfies the following eigenvalue problem

$$-\sum_{i=1}^2 \frac{1}{2r_i^2} \frac{\partial}{\partial r_i} \left(r_i^2 \frac{\partial \Psi}{\partial r_i} \right) + \left(\sum_{i=1}^2 \frac{1}{2r_i} \right) \cdot \left[\frac{1}{\sin \theta} \frac{\partial}{\partial \theta} \left(\sin \theta \frac{\partial \Psi}{\partial \theta} \right) \right] - \sum_{i=1}^2 \frac{2}{r_i} \Psi + \frac{1}{r_{12}} \Psi = E\Psi.$$

The volume of this coordinate is $r_1^2 r_2^2 \sin \theta$. The potential $\frac{1}{r_{12}}$ is expanded as functions on the sphere in θ :

$$\frac{1}{r_{12}} = \sum_{\ell=0}^{\infty} \frac{r_{<}^\ell}{r_{>^{\ell+1}}} P_\ell(\cos \theta), \quad (28)$$

where $r_{>} = \max\{r_1, r_2\}$ and $r_{<} = \min\{r_1, r_2\}$, P_ℓ denotes Legendre polynomial of order ℓ . In the implementation, we truncate the expression (28) into 20 terms and the computational domain from $[0, +\infty)^2 \times [0, \pi]$ to $[0, 5]^2 \times [0, \pi]$. The benchmark energy for the helium atom is set to be -2.903724377 which is taken from [28], at the level of Born-Oppenheimer nonrelativistic ground state energy. The TNN is set to be depth 2 and width 50 in r_1, r_2 and θ and $p = 20$. The boundary

condition is guaranteed by multiplying the subnetwork in the r_i direction with e^{-r_i} . We train the TNN epochs with a learning rate of 1e-04 in the first 100000 epochs and with a learning rate of 1e-05 in the subsequent 50000 steps to produce the final result. The final energy obtained by the TNN method is -2.903781124 and the relative energy error is 1.9542e-05. Figure 9 shows the radial distribution of electrons for helium atoms. From Figure 9, we know that the TNN method can give good simulations of the real electron distribution.

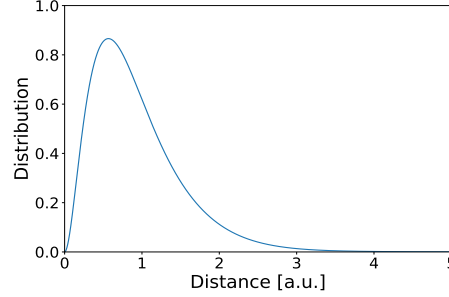


Figure 9: Radial distribution of electrons for helium atom.

5.5 Boundary value problem with Neumann boundary condition

In the last example, different from eigenvalue problems discussed in the above subsections, we tentatively test the performance of TNN for high-dimensional boundary value problems. For this aim, we consider the following boundary value problem with the Neumann boundary condition

$$\begin{cases} -\Delta u + \pi^2 u = 2\pi^2 \sum_{i=1}^d \cos(\pi x_i), & x \in [0, 1]^d \\ \frac{\partial u}{\partial \mathbf{n}} = 0, & x \in \partial[0, 1]^d. \end{cases}$$

Then the exact solution is

$$u(x) = \sum_{i=1}^d \cos(\pi x_i). \quad (29)$$

We use the same loss function as [6] and test cases with $d = 5, 10, 20$, respectively. TNN with depth 2 and width 50 in each subnetwork is used for all cases. Referring to the optimization tips in [27], we use the Adam optimizer in the first 100000 steps and then the L-BFGS in the subsequent 50000 steps to produce the final result. The corresponding numerical results for $p = 2d$ are reported in Figure 10 and Table 5. The final relative errors have almost the same order of magnitude for different dimensions.

From (29), the exact solution can be represented as CP-decomposition with rank d . We can at least claim that the rank of the exact solution is no more than d . For the case $d = 10$, we take hyperparameter p from 1 to 20 and train the TNN with a learning rate of 0.01. Figure 11 shows the final relative errors \hat{e}_{L^2} and \hat{e}_{H^1} after 100000 epochs versus p . From Figure 11, we can find

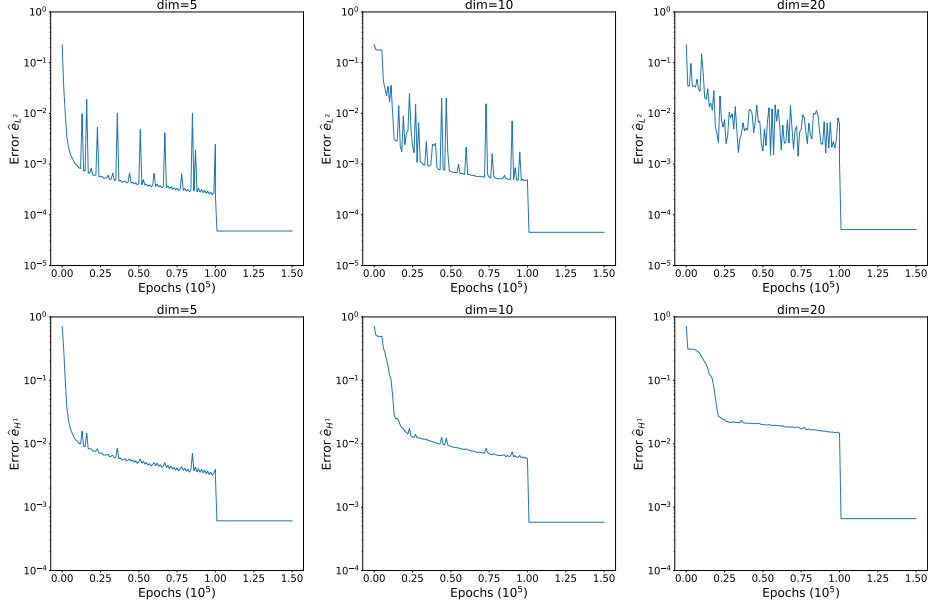


Figure 10: Relative errors during the training process for the Neumann boundary problem: for $d = 5, 10, 20$. The top row shows the relative L^2 errors and the bottom one shows the relative H^1 errors of the approximate solution.

Table 5: Errors of the Neumann boundary value problem for $d = 5, 10, 20$.

d	e_{L^2}	e_{H^1}
5	4.791e-05	6.079e-04
10	4.520e-05	5.778e-04
20	5.122e-05	6.586e-04

an interesting phenomenon that the explicit CP representation (29) may not describe the effect of low-rank approximation properly. From (29), it looks like the real rank of the exact solution is $p = 10$, but there is no significant error reduction from $p = 5$ to $p = 20$.

6 Conclusions

In this paper, we present the TNN and corresponding machine-learning methods for solving high-dimensional PDEs. Different from the well-known FNN-based machine learning methods, TNN has a tensor product form and its numerical integration can use the fixed quadrature points in each dimension. Benefiting from the tensor product structure, we can design an efficient integration scheme for the functions defined by TNN. These properties lead to TNN-based machine learning that can do the direct inner product computation with the polynomial scale of work for the dimension. We believe that the ability of direct inner production computation will bring more

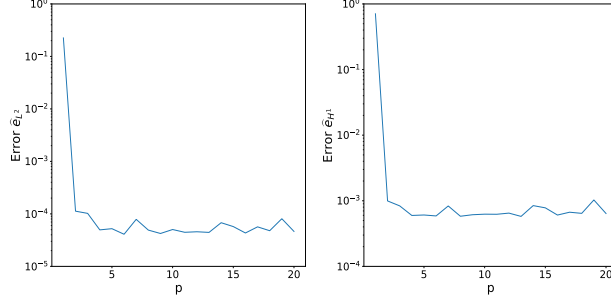


Figure 11: Relative errors vs. hyperparameter p for Neumann boundary value problem ($d = 10$). The left subfigure shows the relative L^2 errors and the right one shows the relative H^1 errors of the approximate solution.

applications in solving high-dimensional PDEs.

Based on the ideas of CP decomposition for tensor product Hilbert space and representing the trial functions by deep neural networks, we introduce the TNN structure, its corresponding approximation property, and an efficient numerical integration scheme. The theoretical results, algorithms, and numerical investigations show that this type of structure has the following advantages:

1. With the help of the straightforward tensor product representation way, we can integrate this type of function separately in the 1-dimensional interval. This is the reason that the TNN can overcome the exponential dependence of the computational work for high-dimensional integrations on the dimension.
2. Instead of randomly sampling data points, the training process uses fixed quadrature points. This means that the TNN method can avoid the random sampling process to produce the GD direction in each step and then has better stability.

Besides above observations, there should exist some interesting topics that need to be addressed in future work:

1. The choice of the subnetwork structure, the activation function, and the more important hyperparameter p .
2. When the computing domain is not tensor-product type, further strategies are demanded to maintain the high efficiency and accuracy of the numerical integration.
3. Since the TNN uses fixed quadrature points, we should design more efficient numerical methods to solve the included optimization problems in the machine learning process.

In addition, more applications to other types of problems should be investigated in the future.

References

- [1] M. Baymani, S. Effati, H. Niazmand and A. Kerayechian, Artificial neural network method for solving the Navier-Stokes equations. *Neural Comput & Applic.*, 26(4) (2015), 765–763.

- [2] G. Beylkin and M. J. Mohlenkamp, Numerical operator calculus in higher dimensions. *Proceedings of the National Academy of Sciences*, 99(16) (2002), 10246–10251.
- [3] A. Beygi, S. P. Klevansky and C. M. Bender, Coupled oscillator systems having partial \mathcal{PT} symmetry. *Phys. Rev. A.*, 91 (2015), 062101
- [4] G. Beylkin and M. J. Mohlenkamp, Algorithms for numerical analysis in high dimensions. *SIAM J. Sci. Comput.*, 26(6) (2005), 2133–2159.
- [5] W. E, Machine learning and computational mathematics. *Commun. Comput. Phys.*, 28 (2020), 1639–1670.
- [6] W. E and B. Yu, The deep Ritz method: a deep-learning based numerical algorithm for solving variational problems. *Commun. Math. Stat.*, 6 (2018), 1–12.
- [7] X. Glorot and Y. Bengio, Understanding the difficulty of training deep feedforward neural networks. In *Proceedings of the thirteenth international conference on artificial intelligence and statistics*, 249–256, 2010.
- [8] I. Goodfellow, Y. Bengio and A. Courville, *Deep Learning*. MIT Press, Cambridge, 2016.
- [9] M. Griebel and J. Hamaekers, Sparse grids for the Schrödinger equation. *M2AN Math. Model. Numer. Anal.*, 41 (2007), 215–247.
- [10] M. Griebel and S. Knapek, Optimized tensor-product approximation spaces. *Constr. Approx.* 16 (2000), 525–540.
- [11] Y. Gu, C. Wang and H. Yang, Structure probing neural network deflation. *J. Comput. Phys.*, 434 (2021), 110231.
- [12] W. Hackbusch and B. N. Khoromskij, Tensor-product approximation to operators and functions in high dimensions. *J. Complexity*, 23(4-6) (2007), 697–714.
- [13] J. H. Halton, On the efficiency of certain quasi-random sequences of points in evaluating multidimensional integrals. *Numer. Math.*, 2 (1960), 84–90.
- [14] J. Han, A. Jentzen and W. E, Overcoming the curse of dimensionality: Solving high-dimensional partial differential equations using deep learning. *arXiv:1707.02568v1*, 2017.
- [15] J. Han, L. Zhang and W. E, Solving many-electron Schrödinger equation using deep neural networks. *J. Comput. Phys.*, 399 (2019), 0021–9991.
- [16] D. Hong, T. G. Kolda and J. A. Duersch, Generalized canonical polyadic tensor decomposition. *SIAM Review*, 62(1) (2020), 133–163.
- [17] K. Hornik, M. Stinchcombe and H. White, Multilayer feedforward networks are universal approximators. *Neural networks*, 2(5) (1989), 359–366.

- [18] K. Hornik, M. Stinchcombe and H. White. Universal approximation of an unknown mapping and its derivatives using multilayer feedforward networks. *Neural networks*, 3(5) (1990), 551–560.
- [19] E. A. Hylleraas, Über den Grundzustand des Heliumatoms. *Z. Physik*, 48 (1928), 469–494.
- [20] P. Jin, S. Meng and L. Lu, MIONet: Learning multiple-input operators via tensor product. *arXiv:2202.06137*, 2022.
- [21] D. P. Kingma and J. Ba, Adam: A method for stochastic optimization. *arXiv:1412.6980*, 2014; Published as a conference paper at ICLR 2015.
- [22] S. Knappek, Hyperbolic cross approximation of integral operators with smooth kernel. Tech. Report 665, SFB 256, Univ. Bonn (2000).
- [23] T. G. Kolda and B. W. Bader, Tensor decompositions and applications. *SIAM Review*, 51(3) (2009), 455–500.
- [24] I. E. Lagaris, A. Likas and D. I. Fotiadis, Artificial neural networks for solving ordinary and partial differential equations. *IEEE Trans. Neural Networks*, 9 (1998), 987–1000.
- [25] I. E. Lagaris, A. C. Likas and G. D. Papageorgiou, Neural-network methods for boundary value problems with irregular boundaries. *IEEE Trans. Neural Networks*, 11 (2000), 1041–1049.
- [26] M. S. Litsarev and I. V. Oseledets, Fast low-rank approximations of multidimensional integrals in ion-atomic collisions modelling. *Numer. Linear Algebra Appl.*, 22(6) (2015), 1147–1160.
- [27] L. Lyu, Z. Zhang, M. Chen and J. Chen, MIM: a deep mixed residual method for solving high-order partial differential equations. *J. Comput. Phys.*, 452 (2022), 110930.
- [28] H. Nakashima and H. Nakatsuji, Solving the Schrödinger equation for helium atom and its isoelectronic ions with the free iterative complement interaction (ICI) method. *J. Chem. Phys.*, 127 (2007), 224104.
- [29] J. Nocedal and S. Wright, Numerical optimization. Springer Science & Business Media, 2006.
- [30] M. Raissi, P. Perdikaris and G. E. Karniadakis, Physics informed deep learning (part I): Data-driven solutions of nonlinear partial differential equations. *arXiv:1711.10561*, 2017.
- [31] M. J. Reynolds, A. Doostan and G. Beylkin, Randomized alternating least squares for canonical tensor decompositions: Application to a PDE with random data. *SIAM J. Sci. Comput.*, 38(5) (2016), A2634–A2664.
- [32] R. A. Ryan, Introduction to tensor products of Banach spaces. London: Springer, 2002.
- [33] J. Shen and H. Yu, Efficient spectral sparse grid methods and applications to high-dimensional elliptic problems. *SIAM J. Sci. Comput.*, 32(6) (2010), 3228–3250.

- [34] J. Shen and H. Yu, Efficient spectral sparse grid methods and applications to high-dimensional elliptic equations II. Unbounded domains. *SIAM J. Sci. Comput.*, 34(2) (2012), A1141–A1164.
- [35] J. Sirignano and K. Spiliopoulos, DGM: A deep learning algorithm for solving partial differential equations. *J. Comput. Phys.*, 375 (2018), 1339–1364.
- [36] Y. Zang, G. Bao, X. Ye and H. Zhou, Weak adversarial networks for high-dimensional partial differential equations. *J. Comput. Phys.*, 411 (2020), 109409.